Quantitative Model for Reversibly Photoswitchable Sensors

Beatrice Adelizzi, Vincent Gielen, Thomas Le Saux, Peter Dedecker, Ludovic
Jullien

HAL Id: hal-03139561

https://hal.sorbonne-universite.fr/hal-03139561v1

Submitted on 12 Feb 2021

Article

Quantitative Model for Reversibly Photoswitchable Sensors

Beatrice Adelizzi,* Vincent Gielen, Thomas Le Saux, Peter Dedecker, and Ludovic Jullien*

Cite This: https://dx.doi.org/10.1021/acssensors.0c02414

Read Online

ACCESS | Metrics & More | Article Recommendations | Supporting Information

ABSTRACT: Composed of a reversibly photoswitchable unit allosterically linked to a sensing module, reversibly photoswitchable sensors (rs-sensors) represent a new and attractive strategy to quantitatively read-out analyte concentrations. However, their kinetic response to illumination is complex, and much attention is required from the design to the application steps. Here, we exploit a generic kinetic model of rs-sensors which enables us to point to key thermokinetic parameters, such as dissociation constants and kinetic rates for exchange toward the analyte, and cross-sections for photoswitching. The application of the model allows to evaluate the robustness of the analyzed parameters and to introduce a methodology for their reliable use. Model and methodology have been experimentally tested on a newly reported calcium sensor based on a reversibly photoswitchable green fluorescent protein allosterically linked to a calcium-sensing module integrating calmodulin and an RS20 peptide.
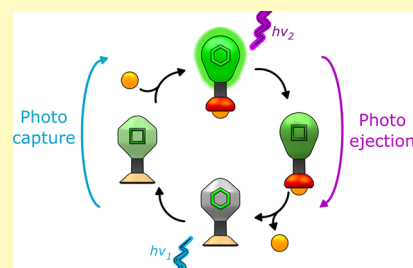
KEYWORDS: biosensors, reversibly photoswitchable proteins, reversibly photoswitchable sensors, calcium sensor, kinetic model

■ INTRODUCTION

Identifying, following, and quantifying specific analytes over time are crucial components in scientific research from material science to cellular physiology. Monitoring complex processes by recording *in situ* the presence of specific ions, molecules, or metabolites requires a synergistic combination of sophisticated chemical tools, advanced sensing technologies, and data analysis. Commonly, the quantification of a targeted analyte relies on measuring the extent of its reaction with a selective sensor. In most protocols, the sensor signal (*e.g.*, fluorescence) is read-out at steady-state to report on this extent. Yet, such a reporting signal depends on the sensor concentration, and it cannot be reliably interpreted for analyte quantification when the sensor concentration is poorly or not even known. This issue is particularly important in living cells where the concentration of genetically encoded sensors is hardly controlled.

This limitation has been overcome in ratiometric sensing by monitoring not one but at least two spectrally shifted sensor signals, the ratio of which eliminates the dependence of the reporting signal on the sensor concentration while retaining its dependence on the analyte's one.[1] An alternative approach to tackle this limitation is to extract the analyte concentration from reading-out the sensor's time-response to a perturbation (*e.g.*, illumination). Indeed, it does not depend on the sensor's concentration. In this regard, the lifetime of fluorescent sensors has been extensively used for sensing various analytes.[2] More recently, the time evolution of the fluorescence signal of reversibly photoswitchable sensors (rs-sensors) upon illumination has enabled analyte imaging with conventional epifluorescence microscopes.[3,4]

The design of rs-sensors relies on a sensing module (*e.g.*, for Ca^{2+}) linked to a reversibly photoswitchable unit (*e.g.*,

reversibly photoswitchable fluorescent protein, RSFP)[5,6] (see insert of Figure 1). In the context of fluorescent, genetically encoded sensors, this last approach is especially attractive since it relies on smaller genes, and sensing does not introduce much bulkiness (unlike chameleon sensors[7,8] that necessitate two spectrally distinct fluorescent units). Moreover, by requiring just a single fluorophore, rs-sensors ensure better performances against issues linked to protein maturation and photobleaching while facilitating their use for multiplexing with other fluorescent probes or optogenetic modulators. Finally, rs-sensors do not require demanding imaging protocols exploiting dual illumination or dual fluorescence collection (as with ratiometric sensing) to access absolute analyte concentration in a way that is largely insensitive to photobleaching.[9]

Nevertheless, rs-sensors exhibit additional features that must be considered for their reliable use. To efficiently report on the complexation state of the rs-sensor (analyte-bound or -unbound), the reversibly photoswitchable unit is allosterically coupled with the sensing module such that the light-driven response of the former is sensitive to the analyte-controlled conformation of the latter. However, this response reflects the realization of multiple reactions. As a consequence, special attention has to be paid to reliably extract the analyte concentration from the time response of an rs-sensor. Furthermore, since allosteric coupling is symmetrical, the photoswitching of the fluorescence unit is anticipated to affect
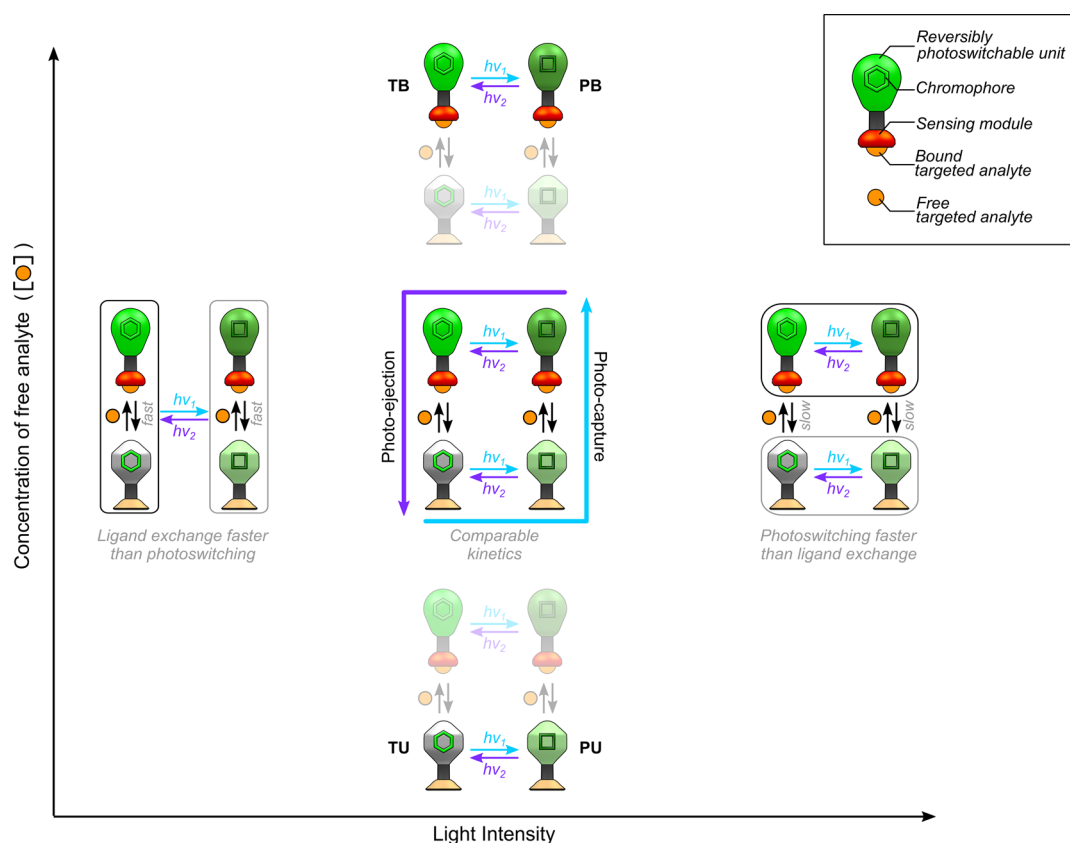
A

Figure 1. Different regimes of an rs-sensor subjected to light-driven read-out. A reversibly photoswitchable sensor integrates two allosterically coupled elements: a module sensing a targeted analyte and a reversibly photoswitchable unit here interconverting a thermodynamically stable state T and a photoactivated state P at two wavelengths λ_1 and λ_2, respectively, promoting $T \rightarrow P$ (cyan arrows) and adding to thermal return $P \rightarrow T$ (violet arrows). Without illumination, the photoswitchable unit of the sensor is in its most favored state T, and its sensing unit is either in its free (TU) or bound (TB) state, provided that the analyte concentration is below or above the dissociation constant $K_{0.5,T}$ of the sensor. Under exposure to illumination, the system is brought out-of-(photo)chemical equilibrium. It evolves to generate a mixture of four analyte-bound and -free T and P states, with composition under control of the analyte concentration ($[L]$) and the eight rate constants associated with the photoisomerizations and analyte exchanges at the steady state. In the most general case, the time response of the sensor signal to a sudden illumination change is complex (central sketch). It can be simplified in asymptotic situations associated with low and high analyte concentrations and low and high light intensities, respectively (peripheral sketches). At low and high analyte concentrations and independently on light intensity, the analyte exchange does not significantly intervene: the time response of the sensor signal can be accounted for with a two-state kinetic model yielding a monoexponential decay, which involves TU and PU on the one hand and TB and PB on the other hand. At a low light intensity, the analyte exchanges are faster than the photoswitching steps, and the generic four-state model reduces at the longest times to a two-state model involving virtual species resulting from averaging over TU and TB or PU and PB: the time response of the sensor signal is monoexponential. At a high light intensity, the time response of the sensor signal is first driven by the kinetics of the photoswitching steps of the analyte-free and -bound states and accordingly biexponentially evolves at intermediate times. Then, it further monoexponentially evolves under control of the kinetics of the analyte exchanges. Since the compositions before illumination and under illumination may differ, photoejection or photocapture of the analyte may intervene at an extent, which depends on the light intensity, analyte concentration, and kinetic window.

the thermodynamics of complexation of the sensing module. As a consequence, the reading-out process may lead to photoejection or photocapture of the sensed analyte (Figure 1).

Therefore, although emerging rs-sensors are promising powerful and versatile tools, their complexity must be thoroughly considered by developers and end users in order to ensure their reliability and acceptance. Upon adopting a recently reported reversibly photoswitchable fluorescent Ca^{2+} sensor, the purpose of this work is to introduce a theoretical frame and a simple methodology enabling to successfully address these issues and precise the parameters, which govern the quantitative interpretation of rs-sensor's signals.

■ RESULTS AND DISCUSSION

Theoretical Perspective. In rs-sensors, light is used both to perturb and read-out the sensor signal. This dual action facilitates implementation, but it rises two significant issues for quantitative and noninvasive analysis. Does the time response of the sensor's signal to light-driven perturbation only depend on the extent of analyte complexation (as in classical titrations)? Does light-mediated reading-out of the sensor's signal introduce a perturbation that may alter the composition of the medium?

The calibration and subsequent use of the sensor relies on parameters extracted from the time response of the sensor signal to a change of illumination (*e.g.*, initial and final values of the sensor signal, time constants). To determine the conditions for reliably extracting these parameters, we adopt a kinetic model of an rs-sensor (Figure 1). This model contains four

states denoted **TU**, **TB**, **PU**, and **PB** (where **T** and **P** stand for thermodynamically stable and photoactivated state, respectively, and **U** and **B** refer to analyte-free and analyte-bound state, respectively) engaged in two photoswitching steps (involving **TU** and **PU**, and **TB** and **PB**) and two analyte exchanges (involving **TU** and **TB**, and **PU** and **PB**). It is first used to examine the protocol of data processing and the significance of the analyzed time range (kinetic window) for extracting the calibration parameters.

Because the working range of the sensor is around the microscopic dissociation constant ($[\mathbf{L}] \approx K_{0.5}$, where $[\mathbf{L}]$ is the analyte concentration), the threshold of light intensities at which photoswitching and analyte exchange occur at the same rate is a fundamental parameter for determining the time response of the sensor's signal. At the threshold, the time response of the sensor's signal to an illumination change is at the most complex and governed by three nonvanishing relaxation times, which are functions of all rate constants of light-driven and thermal reactions (Figure 1, central sketch). In such a situation, the extraction of the calibration parameters by fitting the sensor's time response is poorly reliable and further depends on the processed kinetic window.

In contrast, the time response of the sensor's signal is simplified in asymptotic situations. At light intensities lower than the threshold, the analyte exchanges are faster than the photoswitching steps. The generic four-state model reduces, at the longest times, to a two-state model involving virtual species resulting from averaging over analyte exchanges. In this regime, the response of the sensor's signal to a jump of illumination is monoexponential. Initial and final signal values, as well as the relaxation time, can be reliably retrieved as calibration parameters by fitting over any kinetic window wide enough to observe a significant change of the sensor's signal (Figure 1, left sketch).

In a regime of low light intensities, the measurement may suffer from a low temporal resolution and a low signal-to-noise ratio as a result of slow photoswitching and weak fluorescence emission. These issues are solved at light intensities higher than the threshold albeit upon generating a more complex time evolution of the sensor signal. In this regime, the response of the sensor's signal to a jump of illumination is first driven by the kinetics of the photoswitching steps of the analyte-free and -bound states yielding a biexponential behavior at intermediate times. At a longer time scale, it further monoexponentially evolves under control of the kinetics of the analyte exchange (Figure 1, right sketch). The extent of analyte complexation can now be extracted as a calibration parameter from the biexponential fitting in the kinetic window of intermediate times. To ensure a reliable fit, one should fix the relaxation times associated with photoswitching of the analyte-free and -bound states, which can be extracted from analyzing the monoexponential time responses of the sensor signal at low and high analyte concentrations.

It is of importance to emphasize that the sensor's calibration is valid only for specific values of light intensities. Indeed, the rate constants of the photochemical steps are proportional to light intensity with one-photon excitation, which affects both the amplitudes and the relaxation times of the time response of the sensor's signal (Supporting Information, Appendices A and B). This constrains the calibration to be performed under the same condition of illumination that will be subsequently applied in the experimental routines.

The preceding kinetic model can be as well used to address the issue of changing the medium composition upon reading-out the signal of the rs-sensor. The sensor is initially in its thermodynamically stable state (**T**) and at chemical equilibrium with respect to the analyte exchange. The system composition is dictated by the analyte concentration and the microscopic dissociation constant $K_{0.5,\mathrm{T}}$. In its final steady state, the sensor is distributed in a mixture of **TU**, **TB**, **PU**, and **PB**, and out-of-(photo)chemical equilibrium. In this state, the system composition depends on the analyte concentration ($[\mathbf{L}]$) and on the eight rate constants associated with the photoisomerizations and analyte exchanges (Figure 1 central sketch). When the initial and final distribution of the sensor's states differ, photoejection or photocapture of the analyte is expected at the longest times. While this phenomenon is of no significance when the analyte is in excess of the sensor, it may introduce a significant perturbation when the analyte is at a lower concentration than the sensor (e.g., for the noninvasive analysis of low concentration metabolites in a biological system).

These constraints interestingly level off when illumination causes complete photoactivation of the sensor chromophore (e.g., **T** → **P** and **P** → **T** under the respective wavelengths λ_1 and λ_2; see below) and when the microscopic dissociation constants of the sensor's **T** and **P** states, $K_{0.5,\mathrm{T}}$ and $K_{0.5,\mathrm{P}}$, are similar. In such a case, the composition of the final steady state does not depend anymore on the light intensity, and sensing does not generate any significant release or capture of the analyte. A detailed theoretical analysis is reported in the Supporting Information (Appendices A and B).

Methodology to Calibrate an rs-Sensor. In view of the previous section, the first step for reliably calibrating an rs-sensor is to analyze the time response of its signal under a change of illumination at asymptotic analyte concentrations. Suggested values are $[\mathbf{L}] = 0$ nM and $[\mathbf{L}] \geq 10 \cdot K_{0.5,\mathrm{T}}$, where $K_{0.5,\mathrm{T}}$ can be extracted from titrating the **T** state in the absence of illumination. It is then necessary to define the illumination protocol. When relying on two wavelengths (vide supra), a suggested routine is the alternation of square waves of lights at λ_1 and λ_2 (Figure S1) with the respective intensities carefully selected by taking into account the considerations developed above. Moreover, the kinetic window should be initially fixed by relying on photochemical and kinetic information available from the rs-unit and sensing module in order to ensure that all relaxation processes (photoswitching and analyte exchange) have enough time to occur under illumination.

The calibration step is proposed to first deal with analyzing the monoexponential dependence of the fluorescence time response of the analyte-free and -bound states on the light intensity by performing a series of experiments under illuminations at distinct light intensities. Once the calibration at asymptotic conditions is terminated, one can record the time response of the sensor's signal at intermediate analyte concentrations by using the acquisition conditions set up above and conclude about the asymptotic case in which the measurement is performed. If the observed time response is monoexponential, the photoswitching steps are slower than the analyte exchange. Then, it is possible to exploit the (possibly fitted) initial and final values of the sensor's signal and/or the retrieved relaxation times for preliminary calibration and analyte sensing. Contrarily, if the time response can be accounted by a biexponential function integrating the contributions of the time response of the analyte-free and
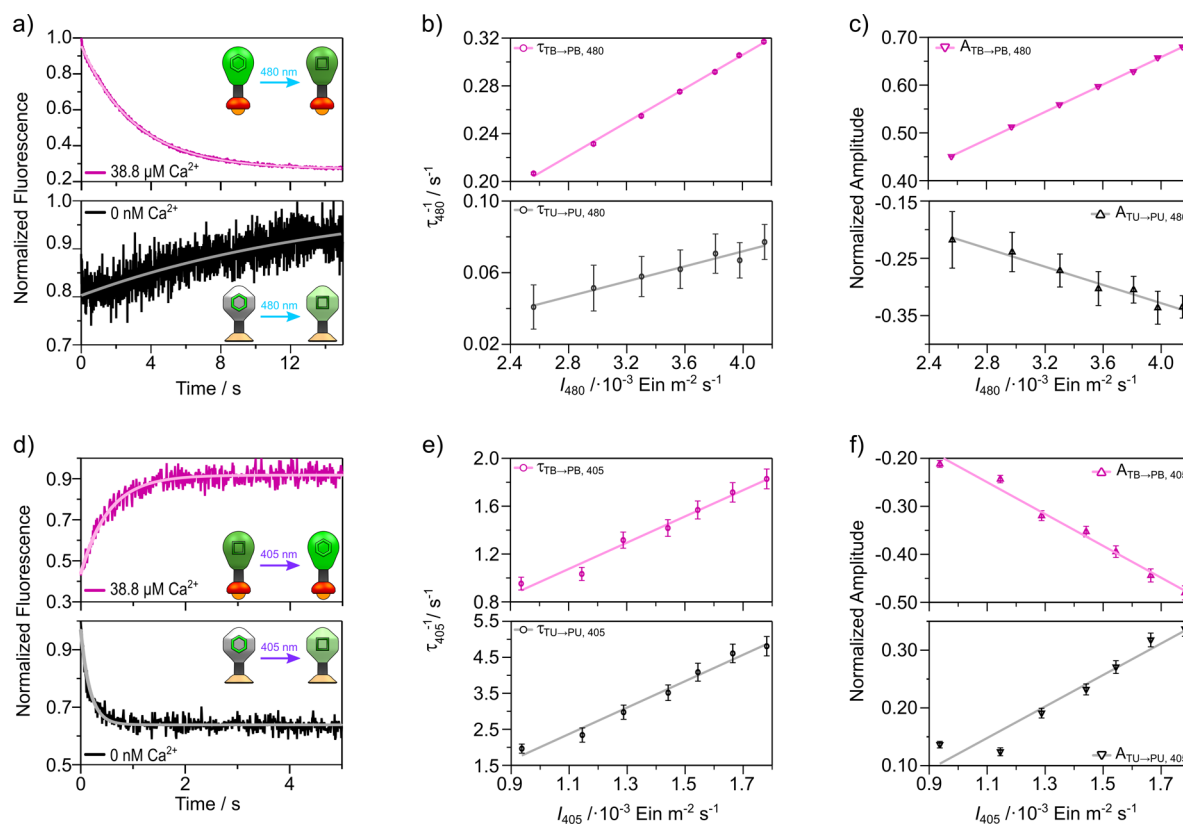
Figure 2. Response of the **GCaMP6s-Q** fluorescence to illumination at 480 (a−c) and 405 (d−f) nm at asymptotic calcium concentrations $[Ca^{2+}]_{\text{free}}$ = 38.8 μM (calcium-bound state; magenta markers and lines) and 0 nM (calcium-free state; black markers and lines). (a,d) Normalized time fluorescence signal recorded at 515 nm. The experimental points are monoexponentially fitted to retrieve the respective relaxation times τ: $\tau_{\text{TB}\rightarrow\text{PB},480}$ (s) = 3.08 ± 0.01; $\tau_{\text{TU}\rightarrow\text{PU},480}$ (s) = 15 ± 2 under I_{480} = 4.15 × 10^{-3} Ein m^{-2} s^{-1}; $\tau_{\text{TB}\rightarrow\text{PB},405}$ (s) = 0.53 ± 0.02; $\tau_{\text{TU}\rightarrow\text{PU},405}$ (s) = 0.179 ± 0.007 under I_{405} = 1.78 × 10^{-3} Ein m^{-2} s^{-1}. (b,e) Dependence of the respective τ^{-1} values on the applied light intensity (markers). The linear fit yields the photoisomerization cross-section σ (from the slope) and an estimation of the rate constant of thermal return $k_{\text{P}\rightarrow\text{T}}^{\Delta}$ (from the intercept with the y axis). (c,f) Linear dependence of the amplitude of the time response of the fluorescence signal on the applied light intensity. (b,c,e,f) Data reported as mean ± sd (n = 3).

-bound states in an appropriate kinetic window, the photo-switching steps are faster than the analyte exchanges. Then, the bound fraction retrieved from the amplitudes of the exponential terms can be used for calibration and analyte sensing (Supporting Information Appendix B).

Therefore, the proposed protocol includes (i) an initial evaluation of the sensor at asymptotic analyte conditions, (ii) the definition of an illumination routine (including the sound choice of light intensity), and (iii) the functional analysis of the fluorescence decay at asymptotic and intermediate analyte concentrations. Depending on how far the time response differs from the monoexponential trend, one can determine the kinetic regime of the sensor (Figure 1) and benefit from a reliable route to calibrate the rs-sensor and extract the analyte concentration. To guide end users to reliably calibrate an rs-sensor, a user-friendly stepwise protocol is reported in the Supporting Information, Section 1.

Experimental Analysis on GCaMP6s-Q. The genetically encoded reversibly photoswitchable calcium sensor recently developed by Dedecker and co-workers,[9] **GCaMP6s-Q**, has been adopted to evaluate the preceding methodology. **GCaMP6s-Q** is a mutant of the established family of calcium-sensing proteins GCaMP, which are composed of a circularly permuted variant of EGFP (enhanced green fluorescent protein) functionalized with a calcium-sensitive moiety integrating a calmodulin (CaM) domain and an RS20

peptide.[10−13] In the presence of calcium ions, CaM and RS20 cooperatively form a ternary complex with four calcium ions triggering a conformational rearrangement of the structure, which causes a rise in fluorescence (Figure S2 and Table S1). Similar to other RSFPs, the rs-unit can be photoswitched between its **T** and **P** states under 480 or 405 nm illumination. Intriguingly, **GCaMP6s-Q** displays opposite photoswitching behavior passing from low to high calcium concentrations. At saturated calcium concentrations ($[Ca^{2+}]_{\text{free}}$ = 39 μM) and under cyan illumination, **GCaMP6s-Q** undergoes positive photoswitching analogous to Dronpa-2;[14] conversely, at $[Ca^{2+}]_{\text{free}}$ = 0 μM, **GCaMP6s-Q** displays negative photo-switching reminiscent of Padron.[15]

Following the above proposed methodology, we first analyzed the time response of the fluorescence signal of **GCaMP6s-Q** solutions at asymptotic calcium concentrations by applying alternate square waves at λ_1 = 480 nm and λ_2 = 405 nm and fixing $[Ca^{2+}]_{\text{free}}$ = 0 nM and = 38.8 μM ([**GCaMP6s-Q**] = 1 μM in 100 mM KCl, 30 mM MOPS (3-(N-morpholino)propanesulfonic acid) in H_2O, pH = 7.2, $[Ca^{2+}]_{\text{free}}$ controlled with a buffer of CaEGTA/EGTA (ethylene glycol-bis(β-aminoethyl ether)-N,N,N′,N′-tetraacetic acid)). Light emitting diodes (LEDs) have been used as light sources to deliver relatively low light intensities (I_{480} = 2.4−4.2 × 10^{-3} Ein m^{-2} s^{-1} and I_{405} = 0.9−1.8 × 10^{-3} Ein m^{-2} s^{-1}).

Under these conditions of illumination, the calcium-bound and calcium-free **GCaMP6s-Q** exhibit contrasting behavior. At $[Ca^{2+}]_{free}$ = 38.8 μM, **GCaMP6s-Q** displays the expected decrease in fluorescence intensity upon illumination at 480 nm. Fluorescence is then recovered by illuminating the solution at 405 nm (Figure 2a,d, magenta traces). At $[Ca^{2+}]_{free}$ = 0 nM, from the second cycle of photoisomerization, **GCaMP6s-Q** exhibits a slow and moderate rise in the fluorescence intensity upon light jump at 480 nm and a fast and intense fluorescence decay under 405 nm illumination (Figure 2a,d black traces).

A series of illuminations at distinct light intensities was performed, and the dependence of the fluorescence temporal response on the light intensity was analyzed (Figures 2b,c,e and 3f). All fluorescence time responses of calcium-bound and calcium-free **GCaMP6s-Q** states have been successfully fitted with monoexponential functions (Figure 2a,d, magenta and black lines), in agreement with a two-state model (Supporting Information, eqs 35 and 66). Hence, we could fix the kinetic windows for further signal acquisition by adopting five times the longest relaxation times extracted at the lowest light intensities (*i.e.*, 20 s for 480 nm-driven forward photoisomerization and 5 s for 405 nm-driven backward photoisomerization).

Moreover, we extracted the sums of the cross-sections of photoisomerization **T** $\rightleftharpoons$ **P** for the bound and unbound states under both 480 and 405 nm illuminations (named as $\sigma_{TB \rightarrow PB,480} + \sigma_{PB \rightarrow TB,480}$; $\sigma_{TB \rightarrow PB,405} + \sigma_{PB \rightarrow TB,405}$; $\sigma_{TU \rightarrow PU,480} + \sigma_{PU \rightarrow TU,480}$; and $\sigma_{TU \rightarrow PU,405} + \sigma_{PU \rightarrow TU,405}$; respectively) from the respective linear dependence of the inverse of the relaxation times (τ^{-1}) on the applied light intensities ($\tau_{TB \rightarrow PB,480}^{-1}$ vs I_{480}, $\tau_{TB \rightarrow PB,405}^{-1}$ vs I_{405}, $\tau_{TU \rightarrow PU,480}^{-1}$ vs I_{480}, and $\tau_{TU \rightarrow PU,405}^{-1}$ vs I_{405}, respectively) (Figure 2b,e, magenta and black markers and lines). The intercept of these linear fits with the *y*-axis under 480 nm illumination further yields an estimate of the rate constant associated with thermal isomerization for the bound and unbound states ($k_{PB \rightarrow TB}^{\Delta}$ and $k_{PU \rightarrow BU}^{\Delta}$), respectively (Supporting Information, eq 33, Table S2).

The relevance of the two-state model for describing the response of **GCaMP6s-Q** calcium-bound and calcium-free states to the illumination enables to derive ranges for the constants $K_{TB \rightarrow PB}^{480}$ and $K_{TU \rightarrow PU}^{480}$ reporting on the photoisomerization extent under 480 nm illumination (Supporting Information, Section 2.2 and Appendix B.1). Upon further considering the linear dependence of the amplitude of the time response of the fluorescence signal on the applied light intensity (Figures 2c,f), we eventually extracted $2.55 \leq K_{TB \rightarrow PB}^{480} \leq 11.96$ and $1 < K_{TU \rightarrow PU}^{480} \leq 3.59$ at I_{480} = 4.15 $\times$ 10^{-3} Ein m^{-2} s^{-1}. From the slope of the respective linear fits, we additionally retrieved the brightnesses of the photoactivated states ($Q_{PB,480}$ = 7960 and $Q_{PU,480}$ = 1925 M^{-1} cm^{-1}) knowing those of the thermodynamically stable ones ($Q_{TB,480}$ = 19,385 and $Q_{TU,480}$ = 1358 M^{-1} cm^{-1}) (Supporting Information, Appendix B.1, Tables S3 and S4).

After terminating the investigation at $[Ca^{2+}]_{free}$ = 0 nM and = 38.8 μM solutions, we recorded the time response of the **GCaMP6s-Q** fluorescence signal to alternate square waves illumination at λ_1 = 480 nm and λ_2 = 405 nm (I_{480} = 4.15 $\times$ 10^{-3} Ein m^{-2} s^{-1} and I_{405} = 1.78 $\times$ 10^{-3} Ein m^{-2} s^{-1}) at intermediate calcium concentrations by using the kinetic window set up above. As expected, by increasing $[Ca^{2+}]_{free}$, the fluorescence temporal evolutions under illumination at 480 and 405 nm show a gradual transition from the trend attributable to the unbound state, **U**, toward the trend related

to the bound state, **B** (Figures 3a,b, and S3). At intermediate $[Ca^{2+}]_{free}$ (especially noticeable at $[Ca^{2+}]_{free}$ = 55−118 nM under 480 nm illumination), the fluorescence temporal evolutions are well-accounted by a biexponential decay upon fixing the time constants to the relaxation times of the calcium-free and -bound **GCaMP6s-Q** states computed from their photoswitching cross-sections (Figure 3a,b). Such behavior can be rationalized as the sum of the contributions of the calcium-free and -bound populations of **GCaMP6s-Q** by assuming the fluorescence change induced by calcium exchange to be rate-limiting (Supporting Information, Sections B.1.2 and B.2.2).

Hence, for **GCaMP6s-Q** calibration, we extracted the dependences of its calcium-bound fraction (θ) on $[Ca^{2+}]_{free}$ from the amplitudes of the biexponential fit of the fluorescence temporal evolution under illumination at 480 and 405 nm (Figures 3c top, S4 and S5). Such dependences were subsequently fitted with a Hill equation to respectively yield $K_{0.5}^{480}$(nM) = 124 $\pm$ 3 and ν_{480} = 2.9 $\pm$ 0.2 and $K_{0.5}^{405}$(nM) = 256 $\pm$ 13 and ν_{405} = 2.4 $\pm$ 0.2. Interestingly, a monoexponential fit of the fluorescence temporal evolutions yields similar results (Figure S4). Originating from an essentially vanishing contribution of the **T** $\rightarrow$ **P** conversion in the calcium-free state of **GCaMP6s-Q**, this can simplify calibration for the end users from directly exploiting the dependence of the fluorescence amplitude on the calcium concentration. This simpler approach has been successfully implemented to demonstrate the relevance of the present processing protocol for applying **GCaMP6s-Q** in living cells (Figure S6).

To further support the conclusion that the fluorescence change induced by calcium exchange is rate-limiting under the investigated condition, we first extracted the analogous **GCaMP6s-Q** calibration curves from analyzing the $[Ca^{2+}]_{free}$-dependence of the initial and final values of the time response of the fluorescence signal to 480 nm illumination $[F_{480}(0), F_{480}(end)]$. As detailed in the kinetic model (Supporting Information Sections B.1.2 and B.2.2), if the calcium exchange is rate-limiting, the Hill parameters retrieved from $F_{480}(0)$ and $F_{480}(end)$ ($K_{0.5,T,480}$ and $\nu_{T,480}$, and $K_{0.5,P,480}$ and $\nu_{P,480}$) should fairly compare with $K_{0.5}^{480}$ and ν_{480} on the one hand and with $K_{0.5}^{405}$ and ν_{405} on the other hand (Figures 3c bottom and S7).

With $100 < K_{0.5} < 250$ nM and $2 < \nu < 3$, all extracted Hill parameters fall in similar range values upon confirming the cooperativity of the binding process. However, we observed a small deviation from the expected trend as $K_{0.5}^{480} \approx K_{0.5,P,480}$ and $K_{0.5}^{405} \approx K_{0.5,T,480}$. We wondered whether this deviation could originate from a too restrictive hypothesis that no calcium exchange occurred within the analyzed kinetic window. To evaluate this explanation, we performed a series of stopped-flow experiments (Figure S8). In particular, we demonstrated that the fluorescence change of **GCaMP6s-Q** associated with calcium exchange takes place at a time scale comparable with the one of photoisomerization at I_{480} = 4.15 10^{-3} Ein m^{-2} s^{-1} and $[Ca^{2+}]_{free}$ = 151 nM (Figure S8c) (τ_{on} = 8 s vs. $\tau_{TB \rightarrow PB,480}$ = 3 s and $\tau_{TU \rightarrow PU,480}$ = 15 s). Such observations further enabled us to extract $1.74 \times 10^{-3} < I_{480} < 4.81 \times 10^{-3}$ Ein m^{-2} s^{-1} and $3.41 \times 10^{-5} < I_{405} < 1.14 \times 10^{-4}$ Ein m^{-2} s^{-1} as orders of magnitude of the range of threshold light intensities at which the rates for the fluorescence changes associated with photoisomerization and calcium exchange are in the same range.

At this point, it is important to notice that the preceding experiments have exploited spatially homogenous illumination
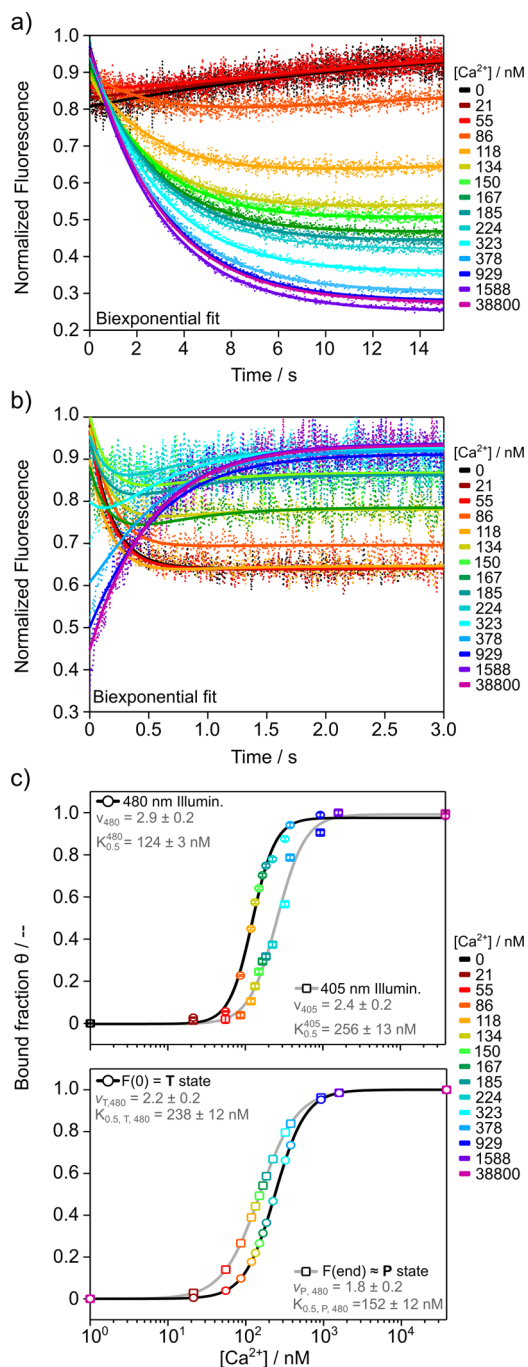
Figure 3. Response of **GCaMP6s-Q** fluorescence to illumination at 480 and 405 nm at intermediate calcium concentrations $[Ca^{2+}]_{free}$. (a,b) Time fluorescence signal recorded at 515 nm under illumination at (a) 480 and (b) 405 nm after normalization by its highest value. The experimental points (dots) were fitted with a biexponential function (lines) to retrieve the calcium-bound fraction θ from the respective amplitudes of the exponential terms upon fixing the relaxation times (a) $\tau_{TB\rightarrow PB,480}$ and $\tau_{TU\rightarrow PU,480}$ and (b) $\tau_{TB\rightarrow PB,405}$ and $\tau_{TU\rightarrow PU,405}$. (c) Dependence of θ on $[Ca^{2+}]_{free}$ as extracted from the amplitudes of the exponential terms under 480 (top, circles and black line) and 405 (top, squares and gray line) nm illumination and from the initial (bottom, circles and black line) and final (bottom, squares and gray line) values of the fluorescence signal under 480 nm illumination. The four dependences (markers) were fitted with a Hill equation (black and gray lines). (c) Data reported as value ± sd, sd calculated from fitting the (a,b) exponentials over the whole range of $[Ca^{2+}]_{free}$. $K_{0.5}$ values in nM.

at rather low light intensities, which is not usually encountered in fluorescence imaging. To further evaluate the relevance of our method for data processing, we measured the fluorescence evolution of **GCaMP6s-Q** in its bound state upon illumination at 480 nm on an epifluorescence microscope at $I_{480} = 0.14$ Ein m^{-2} s^{-1} (40 kW m^{-2}). We extracted 0.07 s for its relaxation time (Figure S9), which is both in line with the expectation from the cross-section measured at lower light intensity and makes **GCaMP6s-Q** appropriate for sensing in epifluorescence microscopy with fast cameras. At an even higher light intensity, **GCaMP6s-Q** fluorescence evolution may be not anymore governed by the photoisomerization of its chromophore but by a thermal step (*e.g.*, the protonation change following the chromophore photoisomerization). This would give rise to a relaxation time in the millisecond range, which would require very fast image acquisition for sensing but would not change the titration protocol to extract the calcium concentration from the amplitudes obtained from the proposed biexponential fit. Another issue could arise in light scanning microscopy. Then, the fluorescence evolution of **GCaMP6s-Q** could be not anymore solely determined by its photochemistry but also by its diffusion, so as to then preferentially apply **GCaMP6s-Q** in fixed samples in order to benefit from the highest spatial resolution.

Eventually, we addressed the issue of photocapture and photoejection, which may be especially significant for a genetically encoded calcium sensor since its working range can be lower than its level of expression. The difference between $K_{0.5,T,480}$ and $K_{0.5,P,480}$ suggests that **GCaMP6s-Q** may be subjected to 480 nm-driven Ca^{2+} photocapture and consecutive 405 nm-driven Ca^{2+} photoejection in the present regime of low light intensities. However, this difference is small and expected to manifest itself only at $[Ca^{2+}]_{free} \approx K_{0.5}$ where $\theta_P \approx 2\theta_T$ (Figure 3c bottom).

■ CONCLUSIONS

This manuscript proposes a theoretical frame and a methodology to ensure an educated characterization and use of the newly introduced class of rs-sensors, which provide an appealing alternative to state-of-the-art sensors. We first introduce a generic kinetic model incorporating noncovalent binding of the analyte to the sensor whose reversible photoswitchable unit photochemically interconverts between two isomeric states. The exploitation of this model points to the significance of the threshold of light intensities at which photoswitching and analyte exchange occur at the same rate. In this way, it allows to determine the optimal experimental conditions to exploit the time response of the sensor's signal to illumination. By enabling the identification of regimes of light intensities and analyzed kinetic windows, the model further allows to reliably extract the analyte concentration. Based on the model, we then propose a simple step-by-step experimental protocol, which provides the kinetic information to calibrate and exploit rs-sensors from robust mono- or biexponential fits after preliminarily analyzing the light-intensity dependence of the time response of the rs-sensor's signal at asymptotic analyte concentrations.

Both the kinetic model and characterization methodology have been applied on the newly reported calcium rs-sensor **GCaMP6s-Q**. In particular, we established that **GCaMP6s-Q** is compatible with illumination promoting essentially complete photoconversions, facilitating its preliminary calibration. Indeed, the initial and final fluorescence signals of its time

response to illumination depend only on the calcium concentration. We further showed that it favorably permits to avoid the introduction of any significant perturbation under calcium sensing.

We expect the kinetic model and the characterization procedure here proposed to be a fruitful support for the sensor developers by guiding them on the fundamental parameters to investigate for the future development of robust and versatile rs-sensors. Analogously, end users will benefit from applying the characterization procedure as it allows for reliable and quantitative analyte measurements.

■ MATERIALS AND METHODS

Materials. Solvents and chemicals were obtained from Aldrich. Kits to produce the calcium solutions buffered at $[Ca^{2+}]_{free} = 0$ and $= 39$ μM were purchased from Thermo Fisher Scientific (both aqueous solutions contain 100 mM KCl, 30 mM MOPS and have pH = 7.2; the solution buffered at $[Ca^{2+}]_{free} = 0$ μM contains in addition 10 mM EGTA; the solution buffered at $[Ca^{2+}]_{free} = 39$ μM contains 10 mM CaEGTA). All home-made solutions were prepared with freshly deionized water from a MilliQ system.

GCaMP6s-Q Production and Purification. Dedecker's plasmid expressing **GCaMP6s-Q** carrying an *N*-terminal hexahistidine tag was transformed in *Escherichia coli* LB21 strain.[9] Cells were grown in Lysogeny broth, and expression was induced at $OD_{600} = 0.6$ by the addition of isopropyl β-d-1-thiogalactopyranoside to a final concentration of 1 mM. Cells were harvested after 16 h of expression at 20 °C by centrifugation (4000*g* for 20 min at 4 °C) and frozen. The cell pellet was resuspended in lysis buffer [phosphate-buffered saline (PBS) buffer: 50 mM phosphate buffer, NaCl 150 mM, and MgCl$_2$ 5 mM, DNAase 5 mg mL^{-1}, phenylmethylsulfonyl fluoride 1 mM, pH = 7.4] and sonicated (5 min at 20% of amplitude, 3 s on, 1 s off). The insoluble material was removed by centrifugation, and the soluble proteins were adsorbed onto Ni-NTA agarose resin suspended in PBS (PBS: Na$_3$PO$_4$ 50 mM, NaCl 150 mM, pH 7.4) *via* overnight incubation at 4 °C under gentle agitation. The protein-loaded Ni-NTA beads were inserted in a column and washed with 20·vol, 50 mM PBS + 20 mM imidazole, 5 mL 50 mM PBS + 40 mM imidazole. Bound proteins were then eluted with 5 mL of 50 mM PBS + 500 mM imidazole. Protein fractions were dialyzed in dialysis cassettes with 2 L of Tris-buffered saline (TBS) buffer [0.1 M TBS buffer (tris(hydroxymethyl)aminomethane), 300 mM NaCl, pH = 7.4] and stored at −20 °C.

GCaMP6s-Q Solutions for Calcium Titration and Photo-isomerization Experiments. Two stock solutions ([**GCaMP6s-Q**] = 8 μM) were prepared by diluting **GCaMP6s-Q** (stored in TBS) with each of the solution of Thermo Fisher kit (*vide supra*). The calcium concentrations of the stock solutions so prepared ($[Ca^{2+}]_{free}$ = 0 and 39 μM) are corrected for the change of the dissociation constant, K_d, of CaEGTA on the ionic strength and on the dilution with **GCaMP6s-Q** storing solutions. The stock solutions were stored at −20 °C for a maximum of 1 month. The operating solutions at asymptotic calcium concentrations ([**GCaMP6s-Q**] = 1 μM and [Ca^{2+}]$_{free}$ = 0 or 39 μM) were prepared by diluting the stock solutions with adequate Thermo Fisher buffer. The operating solutions at intermediate $[Ca^{2+}]_{free}$ were obtained by cross-dilution between the [**GCaMP6s-Q**] = 1 μM solutions at [Ca^{2+}]$_{free}$ = 0 and 39 μM following the procedure described in the Thermo Fisher kit. All operating solutions were freshly prepared for each measurement.

Instruments. Unless stated otherwise, fluorescence measurements for the kinetic analysis were performed in a fluorescence cuvette (1.5 mm optical path) at 20 °C on a LPD220 spectrofluorometer (PTI, Monmouth Junction, NJ) equipped with a TLC50 cuvette holder (Quantum Northwest, Liberty Lake, WA) thermoregulated with a Peltier temperature controller. Light intensities were controlled by varying the current on two LED light sources. The first one (LXZ1-PB01 from Philips Lumileds, San Jose, CA) was filtered at 480 ± 20 nm (HQ 480-40 from Chroma Technology Corp, Rockingham, VT),

whereas the second one (LHUV-0405, Philips Lumileds) was filtered at 405 ± 20 nm (F405-40; Semrock, Rodchester, NY). The LEDs were supplied by a DC4100 LED driver (Thorlabs, Newton, NJ). The two light sources were collimated with ACL2520U condenser lenses (Thorlabs), and the beams were next combined, thanks to a dichroic filter (T425LPXR, Chroma Technology Corp), to deliver homogeneous illumination over the whole sample. The fluorescence temporal evolution upon light jump was followed at 515 nm. Calcium association and dissociation kinetic experiments were acquired on the same instrument equipped with a RX2000 rapid kinetic stopped flow accessory (Applied Photophysics; Leatherhead, UK).

Light intensities were measured by using Dronpa-2 as the external standard by knowing its photoisomerization cross-sections[4] and evaluating the relaxation time (τ) of its fluorescence decay upon photoisomerization at each applied light intensity. This protocol ensures to retrieve accurate values of light intensity at the cuvette under analogous conditions to the performed experiment.

Microscopy experiments were performed in a home-built epifluorescence microscopy setup. The samples were illuminated using a LXZ1-PB01 LED (Philips Lumileds) filtered at 480 nm ± 20 nm (F480-40; Semrock, Rodchester, NY) and a LHUV-0405 LED (Philips Lumileds) filtered at 405 ± 20 nm (F405-40; Semrock, rochester, NY) as light sources. Each LED was supplied by a LED driver (LEDD1B, Thorlabs, Newton, NJ) and modulated synchronously with each other by a waveform generator (33612 A, Keysight Technologies). A lens (ACL2520U; Thorlabs, Newton, NJ, f = 20 mm) was placed just after each diode to collimate the light sources. The two light beams were next combined, thanks to a dichroic mirror (T425LPXR, Chroma, Bellows Falls, VT), and a second pair of lenses was used to focus the light at the back focal plane of the objective after being reflected by the dichroic filter (Di-FF506, Semrock, Rochester, NY). Fluorescence images at 525 ± 15 nm (F525-30; Semrock, Rochester, NY) were acquired for the samples (see below sample preparation) with a 10 × fluar (NA 0.5, Carl Zeiss AG, Feldbach, Switzerland) objective. Objectives were mounted on a home-built microscope equipped with a Luca-R charge-coupled device camera (Andor Technology, Belfast, UK). The bottom surface of the imaged sample was placed on a 0.4 mm thick copper disk in which a hole of 8 mm diameter had been opened for observation with the objective. This metal holder was itself mounted on an aluminum block thermostated at 20 ± 0.2 °C with two thermoelectric Peltier devices (CP 1.0-63-05 L-RTV; Melcor, Trenton, NJ). The stage temperature was maintained at 20 °C with a TCS610 thermistor (Wavelength Electronics, Bozeman, MT), and the feedback loop was driven by a MPT10000 temperature controller (Wavelength Electronics, Bozeman, MT). The samples were submitted to alternate antiphased square wave illumination. Light modulation was performed with two LED sources of λ_{480} and λ_{405} nm with $I_{480} = 0.138$ Ein m^{-2} s^{-1} and $I_{405} = 0.012$ Ein m^{-2} s^{-1}. The angular frequency of modulation was set to 0.5 Hz. Triggering of the camera acquisition was synchronized with the onset of the periodic excitation light (using the option "External start" in the Solis software, Andor Technology). The intensity of the illumination applied to drive the photoisomerization of **GCaMP6s-Q** (in Ein s^{-1} m^{-2}) was calculated by performing a calibration curve with Dronpa-2 as the external standard by knowing its photoisomerization cross-sections and evaluating its photoisomerization decay under the same illumination condition applied.[4] This protocol ensures to retrieve accurate values of the illumination intensity at the sample. The modulated illumination was performed for 10 cycles, and the first cycle was discarded as used just to erase the history of the sample. Cycle no. 2 was used to analyze the photoisomerization kinetics. Following cycles were consistent with cycle no. 2.

Light Jump and Light Titration Experiments. Light jump experiments were performed by applying illumination cycles of square waves at $\lambda_1 = 480$ nm and $\lambda_2 = 405$ nm. Calcium titration experiments relied on four cycles with light intensities $I_{480} = 4.15 \times 10^{-3}$ Ein m^{-2} s^{-1} and $I_{405} = 1.78 \times 10^{-3}$ Ein m^{-2} s^{-1}. The first photoisomerization cycle was used for erasing the sample history, and only the data recorded in the following second, third, and fourth cycles were

analyzed (Figure S1a). Light titration experiments relied on cycles of antiphased square wave lights at λ_1 = 480 nm and λ_2 = 405 nm upon maintaining the light intensity at one wavelength constant throughout the whole experiment and increasing the light intensity of the other wavelength every three cycles (Figure S1b).

Stopped Flow Experiments. Stopped flow experiments were led in a fluorimeter illuminated with the excitation wavelength at minimal light intensity to avoid photoisomerization (λ = 480 nm; I_{480} = 8.3 × 10^{-6} Ein m^{-2} s^{-1}). Using the stopped flow accessory, two 200 μL solutions, A and B, were 1:1 (v/v) mixed with a typical dead time of 30 ms, and the fluorescence intensity at 515 nm was recorded over time at 500 Hz sampling frequency. For the kinetics of association between Ca^{2+} and **GCaMP6s-Q**, we employed (A): [**GCaMP6s-Q**] = 0.5 μM in PBS (sodium phosphate 50 mM, NaCl 150 mM, pH 7.4) and (B): 10 mM CaCl$_2$ in PBS to reach saturated calcium concentration after mixing. 1:1 (v/v) mixing yields [**GCaMP6s-Q**] = 250 nM and [Ca^{2+}]$_{free}$ = 5 mM. Alternatively, (A): [**GCaMP6s-Q**] = 0.5 μM and [Ca^{2+}]$_{free}$ = 0 μM (MOPS buffer containing 10 mM EGTA, pH = 7.2) and (B): [Ca^{2+}]$_{free}$ = 39 μM (MOPS buffer containing 10 mM CaEGTA, pH = 7.2) were employed to reach intermediate calcium concentration after mixing. 1:1 (v/v) mixing yields [**GCaMP6s-Q**] = 250 nM and [Ca^{2+}]$_{free}$ = 151 nM. For the kinetics of Ca^{2+}:**GCaMP6s-Q** dissociation, we employed (A): [**GCaMP6s-Q**] = 0.5 μM, 1 mM CaCl$_2$ in PBS and (B): 10 mM EGTA, 100 mM KCl, 30 mM MOPS in aqueous solutions (pH = 7.2). 1:1 (v/v) mixing yields [**GCaMP6s-Q**] = 250 nM and [Ca^{2+}]$_{free}$ = 13 nM.

Experiments in HeLa Cells. Details of cell culture and protein expression can be found in Gielen et al.[9] For imaging, the cells were rinsed twice and maintained in Hanks' balanced salt solution (HBSS; Invitrogen), supplied with 20 mM N-(2-hydroxyethyl)piperazine-N′-ethanesulfonic acid (HEPES) and 2 g L^{-1} D-glucose (pH 7.4) [HEPES-buffered HBSS (HHBSS)]. Comparable solutions were made with all other components [HHBSS(−)] but without Ca^{2+} and Mg^{2+}. Kinetic traces were exported from imaging experiments performed on the Olympus IX71 microscope (details reported by Gielen et al.[9]). For Ca^{2+} titration, the cells were washed twice and stored in HHBSS(−). Consequently, a 2× stock solution of EGTA/ionomycin was added to the cells to a final concentration of 3 mM EGTA and 5 μM ionomycin. After 10 min of incubation at 20 °C, the buffer was replaced with ionomycin (5 μM) and saponin (0.005%) supplemented with Thermo Fisher buffer for [Ca^{2+}]$_{free}$ = 0 nM. Acquisitions were started immediately. Photoisomerization kinetics was tested with three photoswitching cycles recorded every 90 s. [Ca^{2+}]$_{free}$ was increased every 180 s via cross-dilution of 10 mM CaEGTA buffer (with 5 μM ionomycin and 0.005% saponin) into the Thermo Fisher buffer for [Ca^{2+}]$_{free}$ = 0 nM as described for in-solution experiments. **GCaMP6s-Q** was subjected to a single 100 ms pulse of 405 nm light (I_{405} = 59.3 mW measured at the microscope objective) for on-switching. Kinetics of photoisomerization was then followed by acquiring 10 images under 480 nm light excitation and camera exposure of 100 ms. The analysis reported coincides with the second photoisomerization cycle performed at each [Ca^{2+}]$_{free}$ in line with what reported for in-solution experiments.

ASSOCIATED CONTENT

SI Supporting Information

The Supporting Information is available free of charge at https://pubs.acs.org/doi/10.1021/acssensors.0c02414.

> User-friendly stepwise protocol for the reliable use of rs-sensors, supporting experiments and figures of the experimental results, and an appendix reporting on the theoretical analysis of an rs-sensor (PDF)

AUTHOR INFORMATION

Corresponding Authors

Beatrice Adelizzi − *PASTEUR, Département de Chimie, École Normale Supérieure, PSL University, Sorbonne Université, CNRS, Paris 75005, France;* orcid.org/0000-0002-7763-8999; Email: beatrice.adelizzi@ens.psl.eu

Ludovic Jullien − *PASTEUR, Département de Chimie, École Normale Supérieure, PSL University, Sorbonne Université, CNRS, Paris 75005, France;* Email: ludovic.jullien@ens.psl.eu

Authors

Vincent Gielen − *Laboratory for Nanobiology, Department of Chemistry, KU Leuven, Heverlee 3001, Belgium*

Thomas Le Saux − *PASTEUR, Département de Chimie, École Normale Supérieure, PSL University, Sorbonne Université, CNRS, Paris 75005, France;* orcid.org/0000-0002-2387-2624

Peter Dedecker − *Laboratory for Nanobiology, Department of Chemistry, KU Leuven, Heverlee 3001, Belgium*

Complete contact information is available at:
https://pubs.acs.org/10.1021/acssensors.0c02414

Author Contributions

B.A., T.L.S., and L.J. designed the research and the experiments. B.A. performed the experiments. V.G. and P.D. engineered the protein and contributed with constructive discussion to the research. B.A., T.L.S., and L.J. developed the model and analyzed the experimental results. L.J. and P.D. supervised the research. B.A., T.L.S., and L.J. wrote the manuscript with input from all authors.

Notes

The authors declare no competing financial interest.

REFERENCES

(1) Lee, M. H.; Kim, J. S.; Sessler, J. L. Small molecule-based ratiometric fluorescence probes for cations, anions, and biomolecules. *Chem. Soc. Rev.* **2015**, *44*, 4185−4191.

(2) Szmacinski, H.; Lakowicz, J. R. Fluorescence lifetime-based sensing and imaging. *Sens. Actuators, B* **1995**, *29*, 16−24.

(3) Marriott, G.; Mao, S.; Sakata, T.; Ran, J.; Jackson, D. K.; Petchprayoon, C.; Gomez, T. J.; Warp, E.; Tulyathan, O.; Aaron, H. L.; Isacoff, E. Y.; Yan, Y. Optical lock-in detection imaging microscopy for contrast-enhanced imaging in living cells. *Proc. Natl. Acad. Sci. U.S.A.* **2008**, *105*, 17789−17794.

(4) Wang, P.; Querard, J.; Maurin, S.; Nath, S. S.; Le Saux, T.; Gautier, A.; Jullien, L. Photochemical properties of Spinach and its use in selective imaging. *Chem. Sci.* **2013**, *4*, 2865−2873.

(5) Bourgeois, D.; Adam, V. Reversible photoswitching in fluorescent proteins: a mechanistic view. *IUBMB Life* **2012**, *64*, 482−491.

(6) Zhou, X. X.; Lin, M. Z. Photoswitchable fluorescent proteins: ten years of colorful chemistry and exciting applications. *Curr. Opin. Chem. Biol.* **2013**, *17*, 682−690.

(7) Miyawaki, A.; Griesbeck, O.; Heim, R.; Tsien, R. Y. Dynamic and quantitative Ca^{2+} measurements using improved cameleons. *Proc. Natl. Acad. Sci. U.S.A.* **1999**, *96*, 2135−2140.

(8) Persechini, A.; Lynch, J. A.; Romoser, V. A. Novel fluorescent indicator proteins for monitoring free intracellular Ca^{2+}. *Cell Calcium* **1997**, *22*, 209−216.

(9) Gielen, V.; Mönkemöller, V.; Shen, Y.; Hofkens, J.; Vanden Berghe, P.; Campbell, R. E.; Moeyaert, B.; Dedecker, P. Absolute measurement of cellular activities using photochromic single-fluorophore biosensors. *bioRxiv* **2020**, DOI: 10.1101/2020.10.29.360214.

(10) Chen, T.-W.; Wardill, T. J.; Sun, Y.; Pulver, S. R.; Renninger, S. L.; Baohan, A.; Schreiter, E. R.; Kerr, R. A.; Orger, M. B.; Jayaraman, V.; Looger, L. L.; Svoboda, K.; Kim, D. S. Ultrasensitive fluorescent proteins for imaging neuronal activity. *Nature* **2013**, *499*, 295−300.

(11) Sun, X. R.; Badura, A.; Pacheco, D. A.; Lynch, L. A.; Schneider, E. R.; Taylor, M. P.; Hogue, I. B.; Enquist, L. W.; Murthy, M.; Wang, S. S. H. Fast GCaMPs for improved tracking of neuronal activity. *Nat. Commun.* **2013**, *4*, 2170.

(12) Helassa, N.; Podor, B.; Fine, A.; Török, K. Design and mechanistic insight into ultrafast calcium indicators for monitoring intracellular calcium dynamics. *Sci. Rep.* **2016**, *6*, 38276.

(13) Tian, L.; Hires, S. A.; Mao, T.; Huber, D.; Chiappe, M. E.; Chalasani, S. H.; Petreanu, L.; Akerboom, J.; McKinney, S. A.; Schreiter, E. R.; Bargmann, C. I.; Jayaraman, V.; Svoboda, K.; Looger, L. L. Imaging neural activity in worms, flies and mice with improved GCaMP calcium indicators. *Nat. Methods* **2009**, *6*, 875−881.

(14) Ando, R.; Mizuno, H.; Miyawaki, A. Regulated Fast Nucleocytoplasmic Shuttling Observed by Reversible Protein High-lighting. *Science* **2004**, *306*, 1370−1373.

(15) Brakemann, T.; Weber, G.; Andresen, M.; Groenhof, G.; Stiel, A. C.; Trowitzsch, S.; Eggeling, C.; Grubmueller, H.; Hell, S. W.; Wahl, M. C.; Jakobs, S. Molecular basis of the light-driven switching of the photochromic fluorescent protein Padron. *J. Biol. Chem.* **2010**, *285*, 14603−14609.